Neurodegeneration, Autophagy and Amyloid-beta metabolism in Alzheimer's disease

Abstract: Alzheimer's disease (AD) is a complex neurodegenerative disease presenting with senile plaques, neurofibrillary tangles, extensive cell death, and dysregulation of the cell's internal processes. Out of AD's many molecular hallmarks, we here focus on autophagy's involvement in this pathology. To investigate autophagy's role in AD we studied specifically mouse models with the Swedish and Beyreuther mutations in the *App* gene with either normal or conditional deficient autophagy (due to the knock-out of *Atg7*) in the excitatory neurons (*Atg7* cKO). Using laser microdissection (LMD), we analyzed the proteome of the pyramidal cell layer of CA1 from wildtype, App^{NL-F}, *Atg7* cKO, and *Atg7* cKO x App^{NL-F} mice using label-free mass spectrometry (MS). We initially identified 228 proteins using MS from a LMD CA1 20 µm thickness sample from App^{WT} mice. To increase the number of identified proteins, we established a protocol to cut 30 µm thick CA1 tissue sections. The raw MS results for the whole cohort of mice identified 1130-2046 proteins per mouse. The proteomic analysis showed a significant downregulation of synaptic proteins between *Atg7 cKO x* APP^{NL-F} versus App^{WT}, *Atg7 cKO* versus App^{WT}, *Atg7 cKO x* APP^{NL-F} versus App^{NL-F} mice. Therefore, we next focused on assessing synaptic loss using immunofluorescence (IF), by staining for a specific presynaptic protein, synaptophysin1, to quantify the number of synapses between the mouse groups, until the final MS results arrive. We observed significant differences in the intensity of synaptophysin1 in CA3 between the mouse groups (Welch's ANOVA test $p<0.05$) at 10x magnification and a similar trend but not significant differences comparing the autophagy-deficient and autophagy-competent mice at 63x magnification. The high number of proteins identified by MS can provide a steppingstone for understanding the role of intracellular Aβ and autophagy in AD and for identifying new candidate proteins for the study of AD.

Key words: Alzheimer's disease, autophagy, *Atg7*, mice models, laser microdissection, proteome, CA1, CA3, synaptophysin

Abbreviations:

AD= Alzheimer's disease

APP= Amyloid precursor protein

ATG7= Autophagy related gene 7

Aβ= Amyloid beta

CA1/3= Cornu Ammonis area 1/3

cKO =conditional knock-out

CTF= COOH Terminal Fragment

ELISA= enzyme immunosorbent assay

ER= endoplasmic reticulum

FSB= (*E*,*E*)-1-fluoro-2,5-bis(3-hydroxycarbonyl-4- hydroxy) styrylbenzene

IF= immunofluorescence

IR= infrared

LMD= laser microdissection

MS= Mass Spectrometry

NFT= Neurofibrillary tangles

OCT= optimal cutting temperature compound

Or= oriens layer of the hippocampus CA3 area

PAS= preautophagosomal structure

PEN = polyethylene naphthalate

PET= polyethylene terephthalate

PS1/2= presenilin 1/ 2

Py= pyramidal layer of CA3,

Rad= stratum radiatum,

SLu=stratum lucidum of the hippocampus

TNB= Tris-NaCl-blocking buffer

UV= ultraviolet

WT= wild type

1. Introduction

1.1. Alzheimer's disease

Alzheimer's disease (AD) is a neurodegenerative disease initially described by Alois Alzheimer who had a patient displaying paranoia, confusion, sleep and memory problems. At the autopsy, neuritic plaques consisting of amyloid beta peptide (Aβ) and neurofibrillary tangles (NFT) were observed, which now represent two of the distinctive hallmarks of AD (1). Other hallmarks of AD are: severe synaptic and neuronal loss, neuroinflammation, disrupted axonal traffic, disturbed synaptic vesicles recycling (2), and a disrupted autophagic flux shown by the co-localization of autophagosomes in dystrophic neurites within neuritic plaques (3). While the amount of Aβ and NFT becomes relevant only in the assessment of the later stages of the disease, one good indicator of the advancement of the disease is synaptic loss which can be quantified by immunofluorescence (IF) of well characterized synaptic markers such as synaptophysin1 (1, 4).

One of the most studied pathologies that is associated with AD is Aβ. Aβ comes from the amyloidogenic posttranslational processing of the amyloid precursor protein (APP). APPs are a ubiquitously expressed group of transmembrane polypeptides with a molecular weight of 110-140 kDa, with alternative splicing of the gene's mRNA and posttranslational modifications accounting for the differences in molecular weight (5). Not much is known about the APP's exact functions, but it is speculated that APP is involved in cellular signaling and trafficking (6). APP can undergo proteolytic cleavage both during and after its trafficking in the secretory pathway as a part of its post-translational modifications, however, the specific sites where these cleavages occur are not yet clear. Potential sites of APP processing during the secretory pathway are depicted in **Fig 1** (5,7). Depending on the acting protease, APP can undergo amyloidogenic and non-amyloidogenic processing as shown in **Fig 1** (7). When APP undergoes non-amyloidogenic cleavage, an α-secretase cleaves APP into an sAPP fragment released into the lumen or extracellular space while retaining an 83-residue COOH-terminal fragment (CTF-α) in the membrane. Because the α-secretase cleaves APP withing the Aβ domain, the generation and release of Aβ is prevented. If the APP molecule undergoes amyloidogenic processing, it is cleaved by a β-secretase and the resulting fragments are β-APP and a 99-residue CTF (or CTF-β) (5). CTF99 is further processed by the γ-secretase producing $A\beta_{1-40}$, $A\beta_{1-42}$ at a ratio of 10:1 (7). While most of the produced Aβ is secreted in the extracellular space there is evidence that some of the produced Aβ is catabolized inside the cells (5). Intracellular Aβ is toxic to the cell as it affects the glucose and glutamate transporters, GTP binding proteins, and the function of

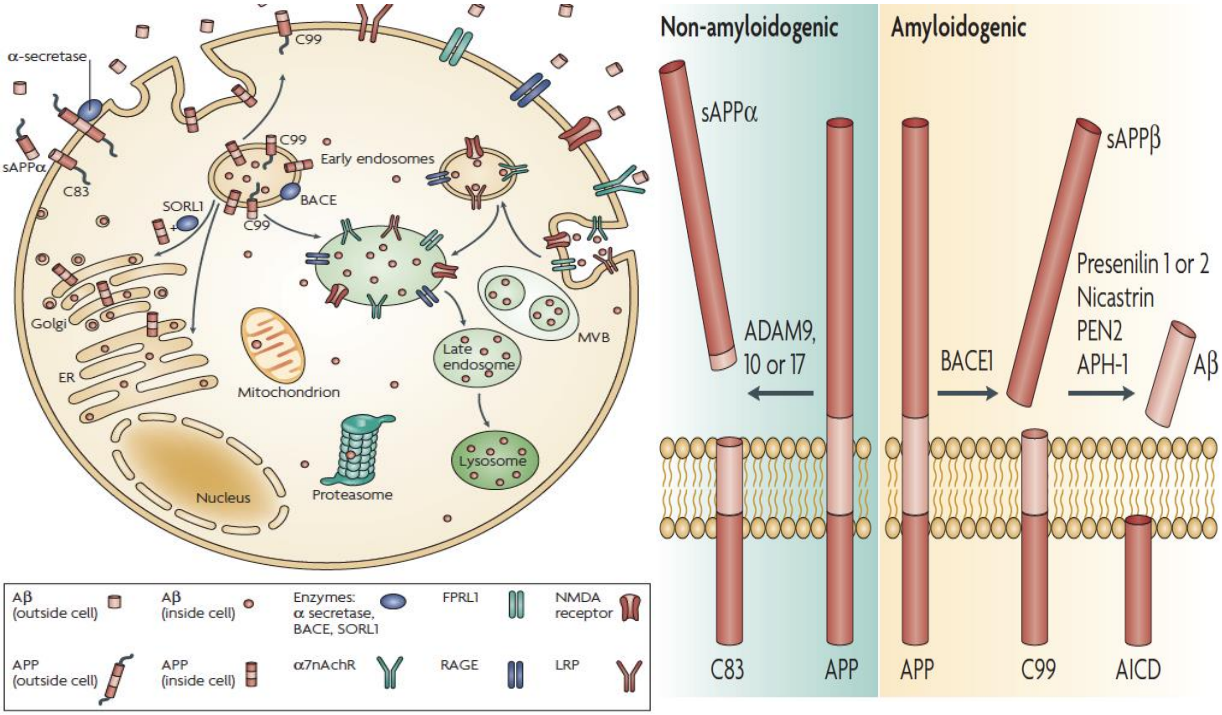

Figure 1: Left panel, the sites of Aβ processing inside the cell during the secretory pathway composed of endoplasmic reticulum (ER), Golgi apparatus, and the vesicles between them (3-7). The Right panel, the two possible routes of APP processing with proposed protein candidates for the α-, β-, and γ-secretase (with PS1 and PS2 among its subunits, and mutations in these subunits result in improper β-APP processing) (2,5,7)

ATPases. Aβ's intracellular effects can translate into a disturbed metabolism and ion homeostasis which can make neurons susceptible to oxidative stress and excitotoxicity (2).

Alzheimer's disease is the most common form of dementia found in people over the age of 65 worldwide and represents over 70% of all dementia cases. However, the multitude of risk factors associated with the disease (increased age, autosomal dominant mutations of the presenilin genes (PS1 and PS2), being female, low education level, and vascular disease) (1, 8) as well as the multitude of hypotheses around the "origin" of AD (the amyloid cascade, prion tau, excitotoxicity, inflammation) (1) combined with the lack of a clear demarcation between dementias, the possibility to definitively diagnose patients only post-mortem, and the inability to stop the progression of the disease, make the research on AD from any angle of approach imperative.

1.2. Autophagy

Autophagy, a process responsible for the degradation and recycling of cellular components was first characterized by Yoshinori Ohsumi in *Saccharomyces cerevisiae* (9). Autophagy is essential

for the maintenance of cellular homeostasis where cellular components are degraded in lysosomes and amino acids recycled. Autophagy is thought to act as a protective mechanism that prevents cell death (10). Autophagic flux, an important term which describes the rate at which a given substrate is cycled through the autophagic process, is often dysregulated in cancer and neurodegenerative diseases such as AD (3).

Depending on the substrate, autophagy can be divided in 3 main types: chaperone-mediated autophagy (where the degradation of cytosolic proteins with the KFERQ motif occurs), microautophagy (where the degradation of non-selectively engulfed cytoplasm occurs), and macroautophagy (where the degradation of protein aggregates and organelles occurs). Macroautophagy is the main process involved in maintaining cellular homeostasis and in this thesis, we will refer to macroautophagy as autophagy (3). Autophagy is a regulated process, requiring the presence of autophagy-related genes (*ATGs*) of which *ATG7* is essential for conventional autophagy to occur (11).

Autophagy begins by the formation of an isolation membrane from a phagophore (a structure potentially derived from ER) which sequesters the organelle destined for autophagy and resulting in a double membrane autophagosome (3). The autophagosome's outer membrane then fuses with a lysosome or late endosome resulting in the formation of an autolysosome. At this stage, the hydrolases contained in the autolysosome are activated by the acidified environment controlled by a proton pump in its membrane. The activated hydrolases digest the contents of the vesicle. After the contents of the vesicle are fully digested, a smaller, denser vesicle containing only hydrolases, called a lysosome is formed (3). A schematic view of the process and its regulatory molecules is depicted in **Fig 2** (12). Similarities between certain lysosomal disorders and AD, for example Niemann-Pick C disease, which shares many pathological characteristics with AD, such as increased burden of waste proteins, dystrophic neurites, amyloidogenic processing of APP, and neurofibrillary tangles point towards the association between autophagy and AD. Secondly, the observation that in AD, autophagic vacuoles accumulate in the dystrophic neurites, co-localizing with senile plaques (3, 13) is another noteworthy link between the two. Other strong indicators that autophagy plays an essential role in AD is the reductions in Aβ plaque and increased perinuclear intracellular accumulation of Aβ in conditional knock-out (cKO) *Atg7* mice (14). In addition, defects in PS1(essential for the lysosomal acidification) result

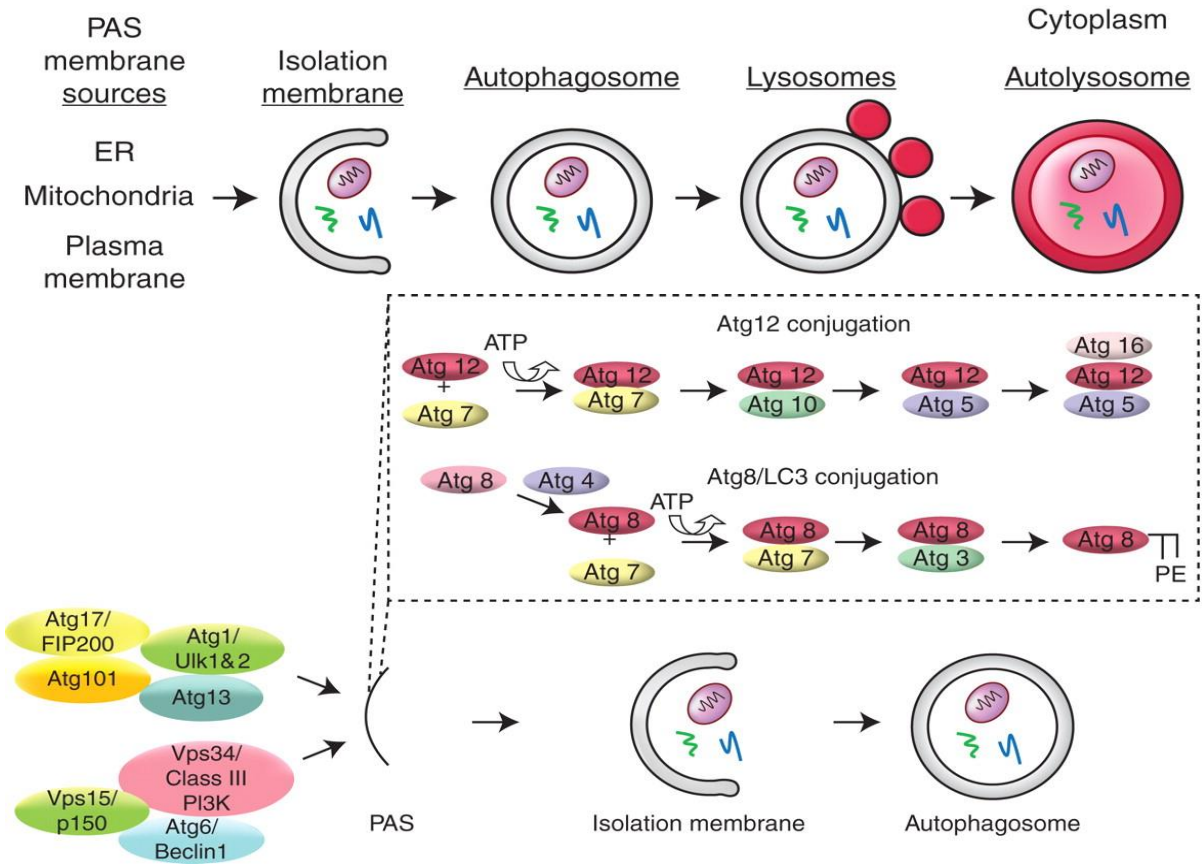

Figure 2: The autophagy pathway: The upper panel shows the general steps of autophagy while the second panel shows the multitude of proteins involved in autophagy and its complexity as a process, with shows the essential role of ATG7 in the formation of the preautophagosomal structures (PAS), indispensable for autophagy to occur (12)

in abnormal levels of autophagy substrates which result in a potential disturbed autophagic flux and cellular homeostasis (3). The stimulatory effect of CTFβ on endocytosis results in an increased rate of substrate delivery and impaired autophagic flux (3). Finally, an upregulation of autophagy occurs in the brains of AD patients at an early stage of the pathology (3).

1.3. Modelling Alzheimer's disease

In this thesis we will use *App* knock-in mice exhibiting the Swedish and the Beyreuther/Iberian (*App*$^{NL-F}$) knock-in mutations with and without the conditional knock-out of *Atg7* in the excitatory neurons of these mice. These mice are obtained according to a protocol described previously and only homozygous mice are used (14, 15). The Swedish mutation (NL) increases the total amount of $A\beta_{1-40}$ and $A\beta_{1-42}$ and the Beyreuther/Iberian knock-in mutation (F) in the *App*$^{NL-F}$ knock-in mice leads to an increased ratio of $A\beta_{1-42}$ to $A\beta_{1-40}$, which is similar to the AD pathology observed in humans (15). These mice models can be used as preclinical disease models for the study of biomarkers of preclinical disease and the cellular phases of AD (16). There are

limitations of this type of disease model such as the different levels in CTFβ and CTFα that may result in unknown artifacts (16).

1.4. Techniques used in this project

a. Laser microdissection (LMD)

Laser microdissection or laser capture microdissection is an advanced microdissection system which combines a high-quality microscope with a laser (which can use ultraviolet (UV), infrared (IR) or carbon dioxide as a source). This system can be used to cut specific cells or small areas of any tissue of choice. The dissectant is collected without contamination risk due to the gravitational forces that pull the dissectant in the collection tube of choice. LMD has numerous applications in genomics and proteomics as it offers an extremely accurate selection of regions or cells of interest. The section of interest (derived from a cryoblock or a paraffin block) is collected on a membrane slide (with the most used ones being polyethylene naphthalate (PEN) and polyethylene terephthalate (PET) depending on the downstream analysis) and stained for subsequent identification under the microscope. The slides are then placed with the membrane facing the collection tube in the microscope's slides holder, and with specific settings, the laser will cut the regions of interest from the section. The regions of interest are selected manually in the software associated with the microscope and through simple commands such as Cut, the laser beam cuts the selected areas of interest, which, after being cut, fall in the collection tube (17). The collected sample can be checked by the microscope by focusing on the collector. After the region of interest is cut and collected, it can be usually stored at -80°C until further downstream analysis is performed.

b. Immunofluorescence (IF)

Immunofluorescence is a subtype of immunohistochemistry technique where the antigen of interest is tagged with a fluorophore instead of being tagged by a chemical reaction that results in the formation of a chromophore. This technique is based on the specific antibody-antigen interaction. There are 2 main types of IF: the direct method, which uses only the primary antibody against the antigen of interest conjugated with a fluorophore and the indirect method which uses an additional secondary antibody against the primary antibody thereby amplifying the detected signal. IF is used to determine the localization of certain proteins and their localized expression in the analyzed tissue. The way the specimen is visualized under the microscope is determined by the specimen's remitted light when illuminated with a short wavelength illumination source. In other words, when the sample is illuminated, light excites the fluorophore

which in turn emits light of a certain wavelength that can then be visualized under the microscope. IF can be used to detect small amounts of antigens.

c. Confocal microscopy

Confocal microscopy eliminates the out of focus light conferring by this way a higher resolution of the image than other techniques such wide field fluorescence microscopy. The out of focus light is eliminated through the insertion of a pinhole at the image plane which makes it impossible for unfocused light to reach the detector. Only the light focused at the pinhole passes. This enhanced focus is possible to be done for one point at a time but to build an image, a scan must be made across the sample in the focused spot. To make this possible, the light beam over the specimen is scanned using 3 mirrors, one for each spatial plane (18). Very precise microscopes use a laser beam instead of a lamp on the sample and allow for various magnifications from 5x to 63x with other additional features to enhance resolution such as air scanning which does that by combining pixel reassignment with the utilization of the rejected light by the pinhole resulting in an improved signal. In this thesis, 10x and 63x images with the Air scanning function for improved resolution are used.

1.5. Hypothesis:

We hypothesize that the genetic deletion of *Atg7* to remove autophagy in excitatory neurons, through conditional knock-out, will induce changes in the proteomic profile between the four groups of mice studied: App^{wt} (wild type), App^{NL-F}, *Atg7* cKO, *Atg7* cKO x App^{NL-F}. We hypothesize we will find significant differences in the expression level of synaptic proteins (shown by the protein score on mass spectrometry (MS)) between these groups, which could account for the more severe observed behavioral deficits found in the *Atg7* cKO mice along with a more severe neurodegeneration phenotype.

1.6. Aims:

The aim of this project is to establish a mechanistic link between autophagy and Aβ metabolism in the neurodegenerative process of AD due to previous observations that autophagy affects both intracellular Aβ and extracellular plaque and that intracellular Aβ is toxic. We aim to characterize our *App* knock-in mice models and especially compare the AD mouse models that are also deficient in autophagy with the AD models competent in autophagy. To investigate this, we set the following objectives of this project:

1. We aim to study how the lack of autophagy affects the proteomic profile of the CA1 neurons of the autophagy-deficient AD mice and to study any downstream effects on the proteome of the intracellular accumulated Aβ in the autophagy deficient AD models.
2. Assess the level of neurodegeneration in these mouse models by comparing the number of synapses in each of the 4 mouse groups using immunofluorescence. This will be done by using synaptophysin1, a presynaptic marker, and quantify its levels in each group.

2. Material and Methods

2.1. Animals used for the experiments

To study the proteome in the neurons from the Cornu Amonis area 1 (CA1) hippocampal area and to investigate the synaptic proteins by immunofluorescence, mice with the following genotypes were used: *App*^{wt}, *App*$^{NL-F}$, *Atg7 cKO x App*$^{NL-F}$, *Atg7 cKO*. For the proteomic analysis, the brain of the mice was embedded in optimal cutting temperature compound (OCT) and kept at -80°C until further use for cryosection. For the immunofluorescence part of this project, the brains of mice of 16-18 months of age were used with the same genotypes as the mice in the proteomic analysis. The sections for immunofluorescence were derived from paraffin embedded brain sections that were cut using the microtome.

2.2. Proteome analysis

a. Cryosection

The brains of the 19-month-old mice from the 4 studied groups are frozen in OCT and kept at -80°C. Prior to cryo-sectioning, the tissue blocks are taken from -80°C and put to -20°C to acclimatize. Then, 30 µm thick sections were cut from the remaining brain hemispheres from another project using Leica3050CM, at -21°C. To maximize the volume of collected tissue, the collection of the sections was done from the most anterior part of the hippocampus that presented the CA1 area until the most posterior part of the hippocampus with the CA1 area as shown in the **Fig 3**. The CA1 area of the hippocampus is chosen for further analysis because it is the area of the brain that is most prone to damage due to neurodegenerative events in AD, so it would be the area where changes in the proteome would be most easily to observe. In addition, since the autophagy-deficient mice lack *Atg7* specifically in excitatory neurons, the CA1 neurons will lack autophagy.

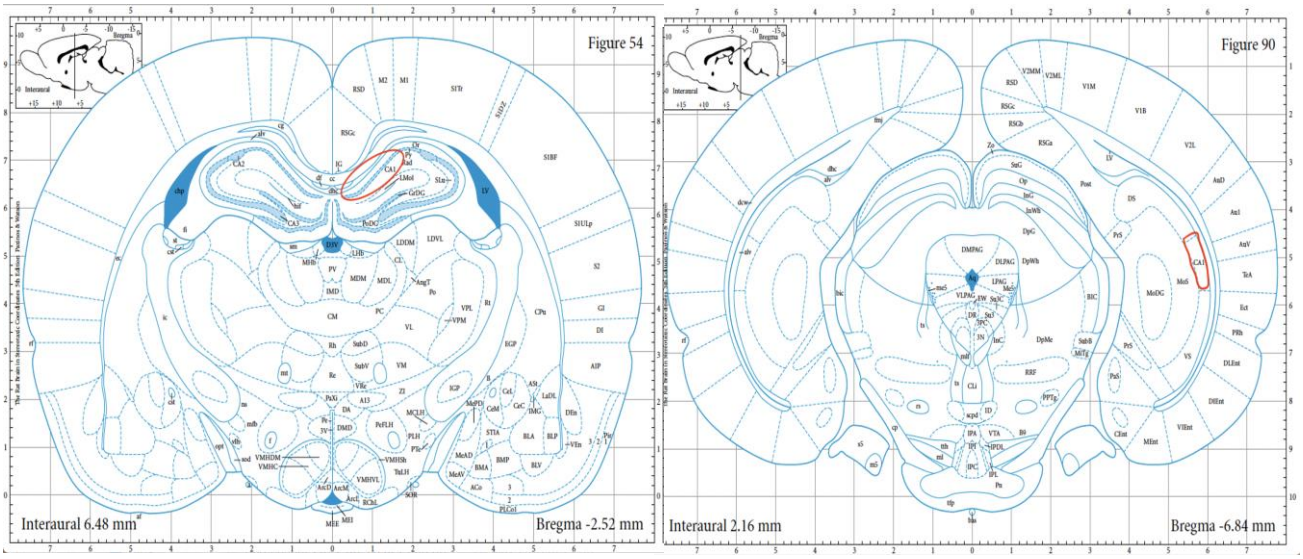

Figure 3: Rat brain sections are shown from a rat brain atlas due to similarity to the mouse brain anatomy. The left panel shows the anterior limit of the hippocampus with the CA1 area marked in red. The right panel shows the posterior limit of the hippocampus with the CA1 area still present. This is indicative of the anatomical margins of collection for the sections sent for MS analysis. The most anterior and posterior margins of the CA1 area were chosen to maximize the volume of tissue collected to maximize the number of identified proteins through label-free MS. (19) Photos from the rat atlas, used due to high similarity with the mouse brain, CA1 area shown in red

b. Staining and collection of samples

The sections were placed on PEN membrane slides (ZEISS, cat no. 415190-9041-000) necessary for subsequent laser microdissection. Prior to LMD, the slides were stained with toluidine blue, according to the following protocol: 3 minutes in ice cold 70% ethanol, a quick wash in deionized H_2O, 30 seconds under toluidine blue staining, and a subsequent 30 second wash of the slide in deionized H_2O. Then the slides were allowed to dry and directly moved to the microscope Leica LMD7000 for microdissection. Before using the PEN slides, they were treated with UV light according to manufacturer instructions for 30 minutes. This is done to enhance the adherence of the tissue to the membrane, improve laser cutting, and sterilize the slides.

c. Laser Microdissection

At the microscope, the specific Leica LMD software is used with optimized settings to cut 30 µm thick CA1 sections. the laser settings depend on the desired thickness of the section, the species, nature of the tissue, its cellular density and components, and its water content. We found that a setting with high pulse frequency, maximum head current, small aperture, low speed, and a power level over 40 give the best cutting results. An equilibrium between optimal cutting that requires little adjustments and does not burn the tissue must be found.

After the CA1 area was isolated from each animal, the tissue from each animal was collected into a tube numbered with an ID unique to each animal and stored at -80°C.

d. Speed vac and preparation of the samples for Mass Spectrometry

The collected samples were pooled, using 10 µL of autoclaved MiliQ water per tube. The samples were dried by speed vac at 1mbar pressure and 2000 rpm speed for 1h, whereafter the samples were kept at -80°C until being shipped to "name of the institution has been redacted for anonymity" for label-free MS. The samples were dried and centrifuged to the bottom of the collection tube.

2.3. Analysis of synaptic puncta

a. Immunofluorescence

For IF, paraffin sections from App^{WT}, App^{NL-F}, *Atg7 cKO x* App^{NL-F}, App^{WT}x *Atg7 cKO* mice are used, with Cornu Ammonis area 3 (CA3) as the area of interest for IF. CA3 is the area of interest because this area is rich in dendrites that synapse with axons coming from the dentate gyrus, also called the mossy fibers. Not only is the CA3 area an area rich in synaptic contacts but it is also a brain region involved in the formation of short-term memory, which is affected due to extensive cellular death occurring in AD resulting in impaired short-term memory, one of the first clinical signs of AD (20). The high presynaptic densities in the CA3 area and its susceptibility to AD make this region perfect for staining with synaptophysin in order to assess the degree of neurodegeneration in these mice models.

On the first day of IF, the paraffinized sections are deparaffinized and hydrated by merging the sections for 5 minutes in xylene (twice), 99% ethanol (twice), 95% ethanol, 70% ethanol, and H_2O. Then, the rehydrated deparaffinized sections are autoclaved at 110°C for 5 minutes in citrate buffer. After the sections are taken from the autoclave, they are gradually cooled down to room temperature and washed in water for 5 minutes and then in 0.05% Tween- PBS (PBST) for 1 minute. The sections are then encircled using a liquid blocker super pap pen. Then 100 µl of TNB (Tris-NaCl-blocking buffer) is added to each slide and the sections are incubated in a humid, dark box at room temperature for 30 minutes, to block unspecific interactions. The sections are then washed with PBST for 5 minutes. After washing, the samples are incubated with 100 µL of Rabbit anti-synaptophysin primary antibody (Rabbit anti-synaptophysin 1 (SYSY cat.101 002)), diluted 1:200 in TNB buffer, except for the negative controls, overnight at +4°C in a dark humid box. The second day, the sections are washed for 3 times, 5 minutes each, with

PBST. All sections are then incubated with 100 µL/slide of secondary antibody (anti-rabbit Alexa 488) for 2 hours at room temperature in a dark humid box. After the incubation time, the sections are again washed 3 times 5 minutes each with PBST and then incubated for 15 minutes with 1:1000 (*E,E*)-1-fluoro-2,5-bis(3-hydroxycarbonyl-4- hydroxy) styrylbenzene (FSB) for Aβ plaque staining. The sections are washed one last time for 5 minutes 3 times and then mounted with Perma Fluor water soluble mounting media (Thermo Scientific). The slides with the cover slips are then dried in the slide holder, protected from light.

b. Confocal microscopy

The third day, the sections are taken to the Zeiss LSM900 Airy microscope. The sections were analyzed at the CA3 area in order to quantify the synaptic puncta number from each animal and compare between the 4 studied groups. In order to do this, we first analyzed the sections at 10X and then at 63X, where we were able to see the presynaptic puncta indicated by positive synaptophysin staining. Laser settings were kept at low values (6% for 10X and 0.8% for 63X to avoid bleaching of the sections but also ensure the detection of a positive signal). The background was established for each animal individually at 63x due to high background differences between the animals. Images at the nearby stratum radiatum (Rad) region of the CA3 area were used as an internal negative control in order to adjust the threshold at 63x in ImageJ to identify true synaptophysin staining and to count the synaptic puncta as accurately as possible.

c. Statistical Analysis

The data from 10x and 63x were analyzed using Brown Forsythe and Welch ANOVA test followed by Dunnett's T3 multiple comparison post hoc test. Outlier and normality tests were also performed.

3. Results

3.1. Summary of results

A first test sample from a wildtype mouse collected with LMD using 20 µm thick sections resulted in the identification of 228 proteins by label-free MS. To increase the number of identified proteins a LMD protocol was established that allowed cutting 30 µm thick tissue sections which enabled the collection of a substantially higher volume of brain tissue sample which was sent for label-free MS analysis. We have successfully identified over 1000 proteins using label-free MS per each animal from each group studied, a significantly higher number of

proteins than in our test sample. The MS analysis of the test sample identified several synaptic proteins, but we are still waiting for the comprehensive analysis of the proteins from our 30 µm thick tissue samples in order to better compare the proteomic profile between the 4 animal groups. To follow with the results from the test sample sent to MS, an in-depth analysis of synaptophysin1, a well characterized presynaptic marker, was performed. We noticed at 10x magnification a significant difference in the intensity of synaptophysin1-positive staining between the studied groups. Significant differences were detected between the App^{WT} and the *Atg7* cKO x App^{NL-F} mice with the hippocampus CA3 regions of the App^{WT} mice being almost 3 times more intense than the same region of the brain in the *Atg7* cKO x App^{NL-F} mouse (Shaphiro Wilcox $p<0.05$, Brown Forsythe and Welch ANOVA $p<0.05$). We also observed significant differences in the intensity between App^{NL-F} and App^{WT}x *Atg7* cKO mice, which exhibited only half of synaptophysin1 intensity in CA3 as compared to App^{NL-F}.
Lastly, a significant difference between App^{NLF} and *Atg7* cKO x App^{NLF} mice was also observed, with the first being more than twice as intense as the latter. At 63x, we observed the same trends.

3.2. Proteome analysis

3.2.1. Test sample results:

First a test sample cut from the CA1 area using LMD App^{WT} mouse brain using 20 µm thick fresh frozen section (2,684,082 μm^2 area and 53,681,640 μm^3 volume respectively), was submitted to MS analysis to get a preliminary estimate on the number of identified proteins. 228 proteins were identified. Interestingly, several synaptic proteins were among the proteins identified (Table 1).

Accession	Description	Score
P11798	Calcium/calmodulin-dependent protein kinase type II subunit alpha OS=Mus musculus OX=10090 GN=Camk2a	67,41
O08553	Dihydropyrimidinase-related protein 2 OS=Mus musculus OX=10090 GN=Dpysl2 PE=1 SV=2	62,60
O88935	Synapsin-1 OS=Mus musculus OX=10090 GN=Syn1 PE=1 SV=2 - [SYN1_MOUSE]	44,56
A0A0J9YUE9	Dynamin-1 OS=Mus musculus OX=10090 GN=Dnm1 PE=1 SV=1 - [A0A0J9YUE9_MOUSE]	40,72
P60879	Synaptosomal-associated protein 25 OS=Mus musculus OX=10090 GN=Snap25 PE=1 SV=1 - [SNP25_MOUSE]	35,62
Q64332	Synapsin-2 OS=Mus musculus OX=10090 GN=Syn2 PE=1 SV=2 - [SYN2_MOUSE]	27,09
O35619	Vesicle associated membrane protein 2 OS=Mus musculus OX=10090 GN=Vamp2 PE=2SV=1[O35619_MOUSE]	21,44
Q9JIS5	Synaptic vesicle glycoprotein 2A OS=Mus musculus OX=10090 GN=Sv2a PE=1 SV=1 - [SV2A_MOUSE]	10,64
P97300	Neuroplastin OS=Mus musculus OX=10090 GN=Nptn PE=1 SV=3 - [NPTN_MOUSE]	10,07
P46096	Synaptotagmin-1 OS=Mus musculus OX=10090 GN=Syt1 PE=1 SV=1 - [SYT1_MOUSE]	8,40
Q5SW88	RAB1A, member RAS oncogene family OS=Mus musculus OX=10090 GN=Rab1a PE=1	6,90

Table 1. *Several synaptic proteins were identified in the test sample, as extracted from the total protein list obtained by MS and sorted by score, the higher the score, the more protein in the sample.*

3.2.2. Sample results from all 4 groups of mice

To investigate the proteome of CA1 pyramidal neurons of App^{WT}, App^{NL-F}, *Atg7* cKO and *Atg7* cKO x App^{NL-F} mice this area was isolated from fresh frozen brain sections with LMD using 10 x magnification lens of the microscope.

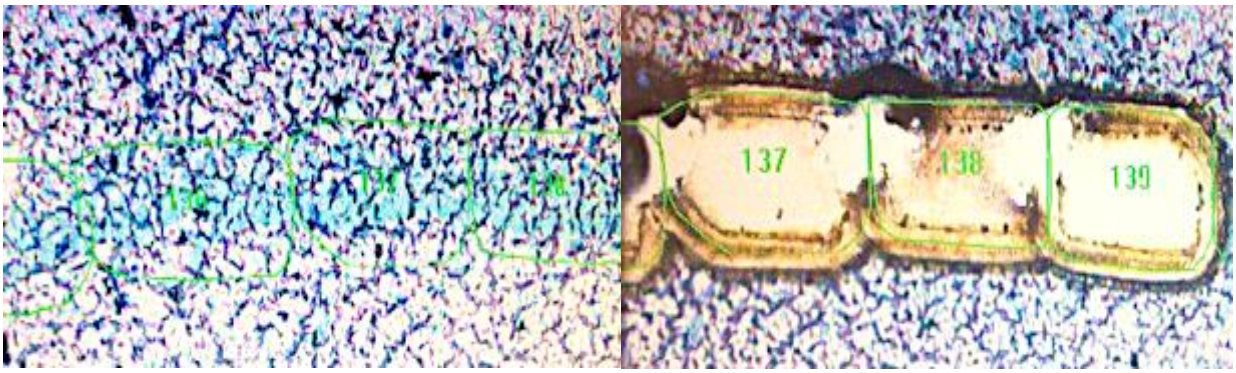

Figure 4: Left panel, CA1 area with marked regions for sectioning; Right panel, CA1 area with marked regions after the tissue has been cut. The figure shows the CA1 area of the hippocampus stained with toluidine blue under 10x magnification at Leica LMD7000. The more stained blue area is the cellular layer of CA1 composed of neuronal soma. This cellular layer is then marked in separate regions which are then cut with the UV laser. The second picture shows the same location of the same tissue after the region of interest has been cut with the laser. Burned margins can be observed at the edges of the remaining tissue and the place where the dissectant has been removed can now be seen.

In order to increase the number of identified proteins, LMD settings were optimized in order to cut 30 µM thick sections. By trying different speeds of the laser cut, intensity and aperture, a successful protocol was established to cut 30 µM thick sections **Fig 4**.

Mouse ID	Genotype	Hemisphere	LMD area (µm²)	Tissue volume* (µm³)
408687	*App^{WT}*	R	5,956,311	178,689,330
18PN13:F7	*App^{WT}*	R+L	2,698,445	80,953,350
18PN13:F8	*App^{WT}*	R+L	6,011,517	180,345,510
408688	*App^{WT}*	R	7,674,593	230,237,790
18PN10:F4	*App^{NL-F}*	R+L	8,087,237	242,617,110
18PN10:F5	*App^{NL-F}*	R+L	3,584,714	107,541,420
18PN14:F2	*App^{NL-F}*	R+L	9,147,081	274,412,430
18PN16:F5	*App^{NL-F}*	R	3,822,759	114,682,770
18PN8:F1	*APP^{NL-F}*	R	2,769,859	83,095,770
18PN11:F4	*Atg7 cKO x APP^{NL-F}*	R	6,212,609	186,378,270
18PN14:F3	*Atg7 cKO x APP^{NL-F}*	R+L	6,995,809	209,874,270
18PN15:F1	*Atg7 cKO x APP^{N-LF}*	R	6,655,226	19,956,780
18PN7:F1	*Atg7 cKO x APP^{NL-F}*	R	4,550,562	136,516,860
18PN17:F3	*Atg7 cKO*	R	5,179,758	155,392,740
18PN18:F1	*Atg7 cKO*	R	7,917,367	237,521,010
18PN18:F2	*Atg7 cKO*	R	2,750,940	82,528,200
18PN20:F2	*Atg7 cKO*	L	7,280,542	218,416,260

***Table 2**: Summary of the CA1 samples collected with cryosection and LMD. R= right, L= left, the volume is calculated by multiplying the total surface of collected tissue from each animal using sections with 30 µm thickness.*

The collected samples were pooled in water and dried with SpeedVac. These samples were sent to the Mass Spectrometry Facility of "name of the institution redacted for anonymity". A summary of the collected tissue samples is shown in Table 2.

After the samples were analyzed using label-free MS, between 1130 and 2046 proteins were identified in each animal as shown in Table 3. An additional animal is added in the *Atg7 cKO x* APP^{NL-F} group (18PN7:F2) from previous sectioning at 20µm thickness and an internal control. The total areas sectioned both in 20µm and 30µm from each animal are shown along with the number of identified proteins per sample.

Sample name	No. id. proteins	Genotype	Total area sent*	Total volume sent
408687	1929	App^{WT}	5,956,311	178,689,330
18PN13:F7	1451	App^{WT}	5,071,250	128,409,450
18PN13:F8	1982	App^{WT}	9,049,742	241,110,010
408688	1970	App^{WT}	7,674,593	230,237,790
18PN10:F4	1951	App^{NL-F}	11,054,868	301,969,730
18PN10:F5	1450	App^{NL-F}	6,575,885	167,364,840
18PN14:F2	1847	App^{NL-F}	12,512,547	341,721,750
18PN16:F5	1747	App^{NL-F}	6,344,989	165,127,370
18PN8:F1	1375	App^{NL-F}	5,114,941	129,997,410
18PN11:F4	1961	*Atg7 cKO x* APP^{NL-F}	9,433,436	250,794,810
18PN14:F3	1996	*Atg7 cKO x* APP^{NL-F}	10,128,365	272,525,390
18PN15:F1	1130	*Atg7 cKO x* APP^{NL-F}	9,036,274	67,577,740
18PN7:F1	1535	*Atg7 cKO x* APP^{NL-F}	7,182,315	189,151,920
18PN7:F2	1350	*Atg7 cKO x* APP^{NL-F}	2,454,048	49,080,960
18PN17:F3	1738	*Atg7 cKO*	7,883,336	209,464,300
18PN18:F1	1930	*Atg7 cKO*	10,513,455	289,442,770
18PN18:F2	1745	*Atg7 cKO*	6,004,947	147,608,340
18PN20:F2	1790	*Atg7 cKO*	9,600,473	264,814,880
Internal control	2046	App^{WT}, App^{NL-F}, *Atg7 cKO x* APP^{NL-F}, *Atg7 cKO*	7,719,923	154,398,460

Table 3: *Final raw data from the label-free MS. In the first column is the sample name or mouse ID with an additional mouse in the Atg7 cKO x* APP^{NL-F} *group and an internal control from previous cutting at 20 µm thickness. On the second column, the number of identified proteins from label-free MS. It is important to note that there is a nonlinear relationship between the number of proteins identified and the amount of tissue. It is also important to note that these data are from the times of cutting the tissue at the microscope and that sample loss could occur during processing the samples for SpeedVac as the sample had to be pooled in one tube and most of it resided on the lid of the tubes. On the third column, the genotype from each mouse is presented and on the last column, the total area for each mouse that was sent for analysis from combining sections of the CA1 area of mice previously cut at 20 µm (from previous work at the laboratory) and then at 30 µm.*

The identified proteins from the mice groups are analyzed by the facility where label-free MS was performed with the following overall results:

1. App^{NL-F} group versus App^{WT} group: 16 proteins were up-regulated in App^{NL-F} group and 24 proteins were down-regulated. Of the significantly modified proteins between these 2 groups, amphiphysin, a protein associated with synaptic vesicles and synapses (21) is observed to be downregulated in the App^{NL-F} group.
2. *Atg7 cKO x* APP^{NL-F} group versus App^{WT} group: 56 proteins were up-regulated in *Atg7 cKO x* APP^{NL-F} group and 74 proteins were down-regulated. Of the synaptic related proteins, neurochondrin, calcium/calmodulin-dependent protein kinase II, spectrin, plasma membrane calcium-transporting ATPase 1, neuroplastin are downregulated in the

Atg7 cKO x APP^{NL-F} group. Another notable downregulated protein is cathepsin D. Upregulated proteins in the *Atg7 cKO x APP*$^{NL-F}$ group include RAB11B but no observed upregulated synaptic proteins.

3. *Atg7 cKO* group versus *App*^{WT} group: 141 proteins were up-regulated in the *Atg7 cKO* group and 184 proteins were down-regulated. Among the identified proteins the synapse associated proteins synaptogyrin-3, Ras related Rab3, synaptic vesicle glycoprotein 2A are upregulated in the *Atg7 cKO* group. Downregulated in the *Atg7 cKO* group are: cathepsin D, along with other synaptic associated proteins such as calcineurin, GRIP-1 associated protein 1, and calcium transporting ATPase.
4. *Atg7 cKO x APP*$^{NL-F}$ group versus *App*$^{NL-F}$ group: 80 proteins were up-regulated in *Atg7 cKO x APP*$^{NL-F}$ group and 93 proteins were down-regulated. Upregulated in the *Atg7 cKO x APP*$^{NL-F}$ group include synaptic related proteins such as SH3 and multiple ankyrin repeat domains protein, Ras-related protein Rab-3, synaptosomal-associated protein 25, t-SNARE coiled-coil homology domain-containing protein. Downregulated in the *Atg7 cKO x APP*$^{NL-F}$ group are plasma membrane calcium-transporting ATPase, spectrin, calcium/calmodulin-dependent protein kinase type II, neurochondrin, which are all associated with synapses and a notable downregulation of cathepsin D is also observed.
5. *Atg7 cKO x APP*$^{NL-F}$ group versus *Atg7 cKO*: 12 proteins were up-regulated in *Atg7 cKO x APP*$^{NL-F}$ group and 16 proteins were down-regulated. Of the significantly modified proteins between these 2 groups, calcium-dependent secretion activator 1 and tenascin, both associated with synapses, are downregulated in the *Atg7 cKO x APP*$^{NL-F}$ group. Interestingly, the RAB11B protein is upregulated in the *Atg7 cKO x APP*$^{NL-F}$ group.

3.3. Synaptic quantification and plaque staining

While awaiting the MS results of the LMD cut CA1, a region rich in synapses as indicated by the preliminary MS data obtained with the test sample, we started analyzing potential changes in the synaptic density in the hippocampus of the autophagy-deficient mice. We chose to stain for synaptophysin1 for which a strong signal was observed in the CA3 region of the hippocampus **Fig 5, 6**. The data shows that a reduction of synaptophysin1 can be observed in the mossy fiber region of the CA3 area in the autophagy deficient mice (*Atg7* cKO and *Atg7* cKO x *App*$^{NL-F}$) as compared to the normal autophagy mice (WT and *App*$^{NL-F}$) both at 10x and 63x. Stained amyloid plaque is also shown in the *App*$^{NL-F}$ and *Atg7* cKO x *App*$^{NL-F}$, just to illustrate the difference in the amount of extracellular amyloid plaque between the models, with the autophagy deficient model presenting with less amyloid plaque **Fig 7**. **Fig 7** is not for the quantification of

the level of plaque, which has been done in another paper (14) but rather just to give the reader the impression of the differences in the extracellular amyloid plaque between the autophagy deficient and competent AD mouse models.

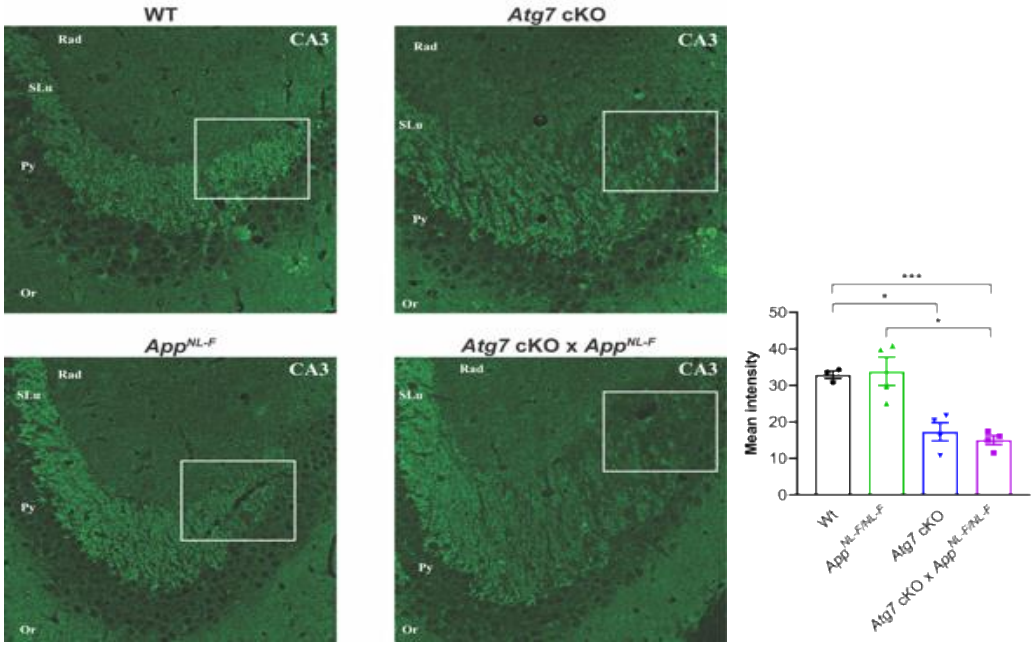

Figure 5: On the left panel, the CA3 area of the mice with positive green staining of synaptophysin1 at 10x. The region of interest is indicated by a white box, where it can be seen a reduction in the positive signal intensity between the mouse groups. Rad= stratum radiatum, SLu=stratum lucidum of the hippocampus, Py= pyramidal layer of CA3, Or= oriens layer of the hippocampus CA3 area. On the right panel, the result of the statistical analysis is presented. Data represent mean ± s.e.m.

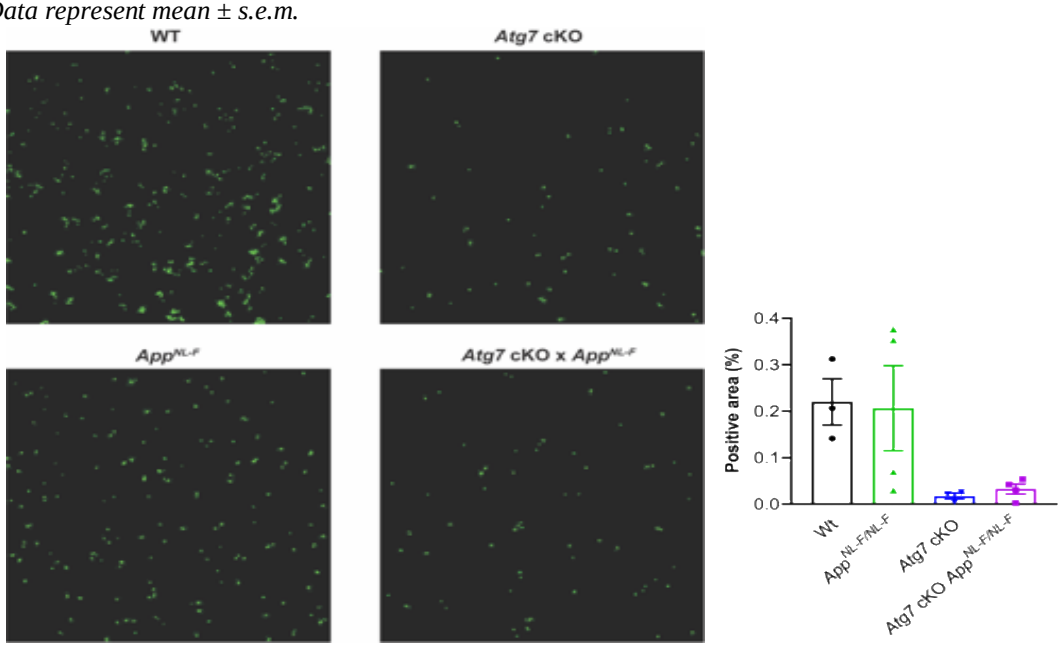

Figure 6: On the left panel, the CA3 area at 63x after thresholding in Image J. The specific area from which the pictures were taken correspond to the area of interest indicated in the white box at 10x in Figure 5. On the right panel, the result of the statistical analysis is presented. Data represent mean ± s.e.m.

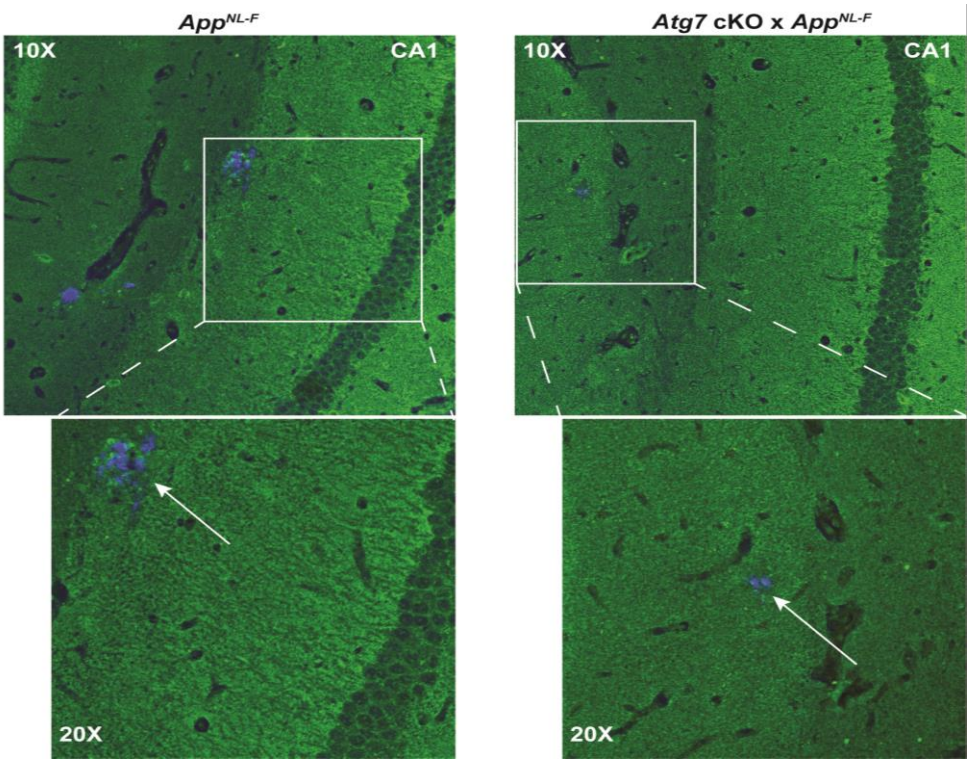

Figure 7: On the top panel, pictures of the CA1 area of the brain from autophagy competent and deficient App^{NL-F} models which show positive synaptophysin1 green staining and positive blue staining of the amyloid aggregates in the neuritic plaque. On the bottom panel, a focus of the indicated region from above in 20x. Here we can see a clearer image of the neuritic plaque indicated by the strong positive blue staining for amyloid beta surrounded by an aggregated stronger synaptophysin1 staining, which just indicates the characteristics of neuritic plaques- accumulation of aggregated extracellular amyloid beta with dystrophic neurites.

4. Discussion

From previous data of Aβ IF staining, we found that there are significantly less extracellular Aβ plaques in the *Atg7* cKO x App^{NL-F} mice as compared to the App^{NL-F} mice (reference to one of the supervisor's current unpublished work, redacted for anonymity). This is paralleled by a pronounced intracellular Aβ accumulation observed in the CA1 pyramidal cell layer of the hippocampus of the *Atg7* cKO x App^{NL-F} mice. AD is characterized by neuronal cell death (1). Interestingly, in this previous study it was observed that cell death was occurring in the CA1 hippocampal layer. During further analysis of apoptosis (through IF of cleaved caspase 3) and necroptosis (through IF of RIPK1) it was found that both of these markers are increased in the CA1 pyramidal cell layer of autophagy deficient mice (reference to one of the supervisor's current unpublished work, redacted for anonymity). Therefore, we hypothesized that cell-death or neurodegenerative processes in this specific region of the hippocampus occur, potentially driven by intracellular Aβ. In order to understand which proteins are involved or significantly changed in this region, we here performed LMD to specifically cut the CA1 pyramidal cell layer

and further analyse the samples by label-free MS analysis to find out potential protein candidates. Interestingly, from our preliminary data from one wild type test sample, we found some synapse associated proteins (shown in Table 1). The dysfunction or lack of these proteins is related with cognitive impairment. Since we observed cognitive impairment in autophagy-deficient mice in our preliminary mouse behaviour data, with the strongest cognitive impairment found in the mouse model with 3 knock-in mutations in the *App* gene and conditional knockout of *Atg7* (reference to one of the supervisor's current unpublished work, redacted for anonymity). This could be due to synaptic alterations in the autophagy-deficient mice. Thus, during the waiting time for the MS data, and based on our preliminary MS data, we performed IF for a typical presynaptic marker synaptophysin1. We chose to analyse a presynaptic marker as the presynaptic terminal might be the origin of the synaptic dysfunction in the *App* knock-in mouse models of AD (22). Interestingly, we found a reduction of synaptophysin1 in the mossy fibers of the CA3 area in the autophagy deficient mice as compared to WT mice. This indicates a presynaptic dysfunction in the hippocampus which might be one of the main reasons for the cognitive impairment in the *Atg7* cKO mice. Since a synapse has both a pre- and postsynaptic component, dual staining with a postsynaptic marker such as PSD95 will be next performed further by the group to establish a more accurate quantification of the synaptic puncta in each animal group studied.

Other than these two synaptic markers, which can be used to quantify synaptic number, the MS analysis might reveal new candidate proteins in the neurodegeneration and synaptic alterations that will be assessed in the near future as we successfully identified between 1130-2046 proteins per mouse.

In continuation with the MS data previously received, the newly received MS data from the full cohort of mice seen in Table 3, was able to identify more than 1000 proteins in each mouse. The downregulated proteins such as neurochondrin (important for spatial learning (23)), calcium/calmodulin-dependent protein kinase II (postsynaptic density with important roles in the regulation of excitatory synapses and synaptic plasticity (24)), spectrin (associated with synapses (25)), neuroplastin (important for long term potentiation in the hippocampus and synaptic plasticity (26)) in the *Atg7* cKO *x* APP^{NL-F} group versus App^{WT} is supported by the IF data that shows a significant decrease in the synapse number of the *Atg7* cKO *x* APP^{NL-F} group when compared with App^{WT} and is in concordance with previous behavioural studies of these mice (reference to one of the supervisor's current unpublished work, redacted for anonymity).

The interesting upregulation of synaptogyrin-3, associated with the presynaptic vesicles, in the *Atg7 cKO* group versus App^{WT} might explain some of the neurodegenerative effects produced by knocking-out autophagy as it has been observed that lowering synapotgyrin-3 in mice has the potential to rescue the tau induced memory deficits in mice (27). The downregulation of calcineurin (important in synaptic plasticity and memory (28)) as well as GRIP-1 associated protein 1 (involved in long term potentiation (29)) and calcium transporting ATPase (found in synaptic vesicles (30)) support the significantly decreased synaptic number found by IF in the CA3 area of the brain between the *Atg7* cKO group versus App^{WT}. The downregulation of synaptic proteins in the *Atg7* cKO *x* APP^{NL-F} group versus App^{NL-F} such as plasma membrane calcium-transporting ATPase (associated with synapses (30)), spectrin (25), calcium/calmodulin dependent protein kinase type II (synaptic plasticity, memory formation (24)), and neurochondrin (important for spatial learning (23)) is corroborated by the significant decrease in synaptic number shown by IF in the *Atg7* cKO *x* APP^{NL-F} when compared with App^{NL-F} as well as previously done behavioural studies in these mice in the research group, with the autophagy deficient mice showing a much more accentuated pathology. The downregulation of tenascin, a protein found in the perineural network that influences long term potentiation (31), might also explain the accentuated pathology phenotype observed in the *Atg7* cKO *x* APP^{NL-F} when compared with *Atg7* cKO.

Other notable proteins that are observed to be modified between the mouse groups are cathepsin D and RAB11B, both with functions around the amyloid beta metabolism (31, 32). Cathepsin D is involved in Aβ degradation while RAB11B controls beta-secretase endosomal recycling of APP and consequent cleavage of APP into CTF99 which is further processed by gamma secretase into amyloid beta (32,33).

The downregulation of cathepsin D in *Atg7* cKO *x* APP^{NL-F} group versus App^{WT} along with the upregulation of RAB11B might confer arguments in support of the imbalance in protein substrates (here APP and its derivatives) that can affect the autophagic flux, which is dysregulated in AD (3). The downregulated cathepsin D is observed when comparing all groups that are deficient in autophagy with the autophagy competent models (*Atg7* cKO *x* APP^{NL-F} group versus App^{WT}, *Atg7* cKO group versus App^{WT}, *Atg7* cKO *x* APP^{NL-F} group versus App^{NL-F}) which might explain the previous obtained data that apoptosis (through IF of cleaved caspase 3) and necroptosis (through IF of RIPK1) are increased in the CA1 pyramidal cell layer of autophagy deficient mice (reference to one of the supervisor's current unpublished work, redacted for

anonymity) as cathepsin D is also involved in apoptotic and necroptotic cellular processes, but it is too early in the analysis of the data process to say this with certainty (34).

4.1. Proteome analysis

Through literature studies and optimization of the LMD protocol, we established conditions to cut 30 µm thick sections. Through label-free MS we have therefore obtained over 1000 proteins from each mouse from the studied cohort. This is according to our expectations as we expected to identify a higher number of proteins by label-free mass spectrometry as the volume of sample obtained this time is larger than what was sent as a test sample. Moreover, the label-free MS data support some of our previous findings such as: a decreased in synapse number between certain mouse models corroborated by a downregulation of synaptic proteins in the MS study and a more pronounced pathologic phenotype in behavioral studies of these mice, dysregulations in proteins involved in amyloid-beta metabolism such as cathepsin D and RAB11B which might shed some light over how autophagy deficiency affects amyloid beta metabolism and results in an accumulated perinuclear Aβ and reduced extracellular plaque, and also can contribute to support the previous findings, although it is too early in the analysis of the data process, of increased apoptosis and necroptosis in the *Atg7* cKO models when compared with the autophagy competent ones in the CA1 area.

4.2. Synaptic quantification

Single staining for quantification of synapses proves to be challenging, especially if the focus is to study particular discrete differences between groups. Single staining with either a presynaptic or postsynaptic marker poses a challenge in quantifying the number of synapses as the difficulty of setting a threshold in ImageJ for identification of a true signal is very hard to overcome. Not only this, but also the different background given from each animal which makes setting a threshold for identifying true signal and not lose information even more difficult. This matter becomes more accentuated at higher magnifications. One solution we employed was to make an internal negative control for each animal analyzed at 63x with using the Rad region, a region in the vicinity of the molecular layer of CA3 which does not stain positive for synaptophysin1 and hence provides a good indicator of unspecific staining. Thresholds were set for each animal using the Rad nonspecific staining as negative controls to adjust these thresholds. Using this protocol, we were able to show a decrease of synaptophysin in the CA3 region upon autophagy-deficiency showing that autophagy plays a role in synaptic maintenance **Fig 5, 6**.

Another solution to overcome these problems is to employ double staining, by staining a presynaptic and a postsynaptic marker and quantify the co-localization of these 2 signals as one synapse (35). Many existing software are available to quantify synaptic puncta if one performs dual staining.

To address the lack of finding significant differences between the groups, besides double staining, one could also increase the number of animals analyzed in each group as well as the number of sections that have to be stained. By increasing the n number of each group analyzed, one could increase the chances of finding significant differences between the groups at a higher magnification.

We have employed here the analysis of the CA3 area due to its high number of presynaptic contacts as well as heavily involvement in clinical AD (20). This analysis of synaptic puncta could be extended to the CA1 area, which we plan to do in the future, as this area is rich as well in presynaptic contacts. This further analysis that would include the CA1 area can be also supported by the already available label-free MS data and can present a much more comprehensive image of synaptic loss that occurs in our mice models along with the other molecular and behavioral phenomena already observed in our mice groups.

4.3. Conclusions

Here we successfully established an LMD protocol to isolate the CA1 pyramidal layer from AD mouse models. The analysis of the LMD cut tissue from a test sample by MS identified more than 200 proteins, including several synaptic proteins. One of them, synaptophysin was shown to be decreased by IF in CA3 mossy fibers of autophagy-deficient mice. Hence, the label-free MS results from CA1 pyramidal cell layer will contribute to elucidating the effects of intracellular Aβ and point towards the study of other protein candidates involved in AD pathology and autophagy deficiency as our results from the most recent sent LMD CA1 samples identified over 1000 proteins from each mouse in the studied cohort, some of which contribute to corroborate the previous findings of the research group.

The significant reduction observed in the presynaptic marker synaptophysin1 in autophagy deficient mice in the CA3 area indicates that there is a presynaptic dysfunction that occurs in the autophagy deficient mouse hippocampus which might be one of the reasons for mouse cognitive impairment in the *Atg7* cKO mice. This reduction in synaptic numbers is also corroborated by MS data that shows a downregulation of synaptic markers in the *Atg7* cKO mice as well as cathepsin D which is linked to apoptotic and necrotic processes.

5. Appendix

5.1. Ethical reflections

In this project, research work involves mice, so it is imperious that the 3Rs of ethical research are respected. Replace, which involves the replacement of mice with another research model (for example, cell cultures) is not possible as the experiment is centered around analyzing different aspects of neurodegeneration at the system level in the aging brain, parts of the experiment involving the analysis of specific matured anatomical areas such as the CA1 and CA3 area of the hippocampus, the areas of the brain most susceptible to neurodegenerative events. Reduction is respected as the minimum number of mice is used to obtain a significant statistical analysis with enough power (n=4/5). The principle of refinement is also respected as the mice were kept in good condition at "name of the institution has been edited for anonymity" and under the ethical approval with the number "number has been edited for anonymity". The animals were controlled by animal technicians and euthanatized in humane conditions, after which their brain was isolated and used for further experiments.

5.2. Motivation of methods

Currently LMD is the only method one can employ when trying to precisely section very specific areas of a solid tissue. There are alternatives to LMD such as fluorescence activated cell sorting, and manual cell picking. LMD was used here to provide continuity with an ongoing project and due to previous knowledge and experience in the group. FACS was excluded as a technique because we wanted to keep the cell-cell interactions in the tissue architecture available for downstream study as we do not currently know how the dissociation of the cells from the tissue architecture would affect any downstream analysis. Manual cell picking is extremely lucrative and better results with the same manual selection can be performed using LMD (36).
Alternatives to immunofluorescence are immunohistochemistry and other protein analysis methods such as Western blot and enzyme-linked immunosorbent assay (ELISA). It is usually best to support the findings of IF with Western blot and/or ELISA whenever possible. Here we chose IF because it is a simple, specific, and sensitive method that allows for tagging of multiple proteins when compared with immunohistochemistry, that while it does not have the risk of having bleached slides, it has other challenges such as no staining (due to for example unproperly unmasking the epitope that has to be tagged), variable penetration of the antibody to the epitope for proper staining when trying to unmask the epitope by various techniques etc.
We chose label-free mass spectrometry as we have very little sample and choosing an isotope-based MS method would result in further loss of the material during labeling.

For the initial study and quantification of the synaptic puncta, a confocal microscope at 63x was the fit choice as it provided the perfect balance for the ability to count the synaptic puncta and the availability of protocols on how these puncta can be quantified.

ACKNOWLEDGEMENTS

I would like to express my great appreciation to my direct supervisor "name has been edited for anonymity" for his valuable and constructive suggestions during the planning and development of this project. His willingness to give his time so generously has been very much appreciated. I also want to thank "name of the other supervisor has been edited for anonymity" for his guidance and openness to teach practical as well as theoretical concepts for the study of Alzheimer disease using mice mouse models and various research techniques.

Total word count excluding only references: 8727.
Total word count according to guidelines: 7598.

References:

1. Castellani R, Rolston R, Smith M. Alzheimer Disease. Disease-a-Month. 2010;56(9):484-546.
2. Mattson M. Addendum: Pathways towards and away from Alzheimer's disease. Nature. 2004;431(7004):107-107.
3. Nixon R, Yang D. Autophagy failure in Alzheimer's disease—locating the primary defect. Neurobiology of Disease. 2011;43(1):38-45.
4. Rehm H, Wiedenmann B, Betz H. Molecular characterization of synaptophysin, a major calcium-binding protein of the synaptic vesicle membrane. The EMBO Journal. 1986;5(3):535-541.
5. Selkoe D. Alzheimer's Disease: Genes, Proteins, and Therapy. Physiological Reviews. 2001;81(2):741-766.
6. Nixon R. Autophagy, amyloidogenesis and Alzheimer disease. Journal of Cell Science. 2007;120(23):4081-4091.
7. LaFerla, F., Green, K. and Oddo, S., 2007. Intracellular amyloid-β in Alzheimer's disease. *Nature Reviews Neuroscience*, 8(7), pp.499-509.
8. Drummond E, Wisniewski T. Alzheimer's disease: experimental models and reality. Acta Neuropathologica. 2016;133(2):155-175.

9. Takeshige K, Baba M, Tsuboi S, Noda T, Ohsumi Y. Autophagy in yeast demonstrated with proteinase-deficient mutants and conditions for its induction. Journal of Cell Biology. 1992;119(2):301-311.
10. Choi, A., Ryter, S. and Levine, B., 2013. Autophagy in Human Health and Disease. *New England Journal of Medicine*, 368(7), pp.651-662.
11. ARAKAWA, S., HONDA, S., YAMAGUCHI, H. and SHIMIZU, S., 2017. Molecular mechanisms and physiological roles of Atg5/Atg7-independent alternative autophagy. *Proceedings of the Japan Academy, Series B*, 93(6), pp.378-385.
12. Das, G., Shravage, B. and Baehrecke, E., 2012. Regulation and Function of Autophagy during Cell Survival and Cell Death. *Cold Spring Harbor Perspectives in Biology*, 4(6), pp.a008813-a008813.
13. Boland B, Kumar A, Lee S, Platt F, Wegiel J, Yu W et al. Autophagy Induction and Autophagosome Clearance in Neurons: Relationship to Autophagic Pathology in Alzheimer's Disease. Journal of Neuroscience. 2008;28(27):6926-6937.
14. this citation has been redacted for anonymity
15. this citation has been redacted for anonymity
16. this citation has been redacted for anonymity
17. [Internet]. Downloads.leica-microsystems.com. 2021 [cited 17 May 2021]. Available from: https://downloads.leica-microsystems.com/Leica%20LMD7000/Brochures/Leica_LMD6500-7000-Brochure_en.pdf
18. St. Croix, C., Shand, S. and Watkins, S., 2005. Confocal microscopy: comparisons, applications, and problems. *BioTechniques*, 39(6S), pp.S2-S5.
19. Paxinos, G. and Watson, C., n.d. Paxinos and Watson's the rat brain in stereotaxic coordinates. Elsevier Academic Press.
20. Basu, J. and Siegelbaum, S., 2015. The Corticohippocampal Circuit, Synaptic Plasticity, and Memory. *Cold Spring Harbor Perspectives in Biology*, 7(11), p.a021733.
21. Lichte B, Veh R, Meyer H, Kilimann M. Amphiphysin, a novel protein associated with synaptic vesicles. The EMBO Journal. 1992;11(7):2521-2530.
22. Hark T, Rao N, Castillon C, Basta T, Smukowski S, Bao H et al. Pulse-Chase Proteomics of the App Knockin Mouse Models of Alzheimer's Disease Reveals that Synaptic Dysfunction Originates in Presynaptic Terminals. Cell Systems. 2021;12(2):141-158.e9.
23. Ncdn - Neurochondrin - Mus musculus (Mouse) - Ncdn gene & protein [Internet]. Uniprot.org. 2021 [cited 17 June 2021]. Available from: https://www.uniprot.org/uniprot/Q9Z0E0

24. Colbran R, Brown A. Calcium/calmodulin-dependent protein kinase II and synaptic plasticity. Current Opinion in Neurobiology. 2004;14(3):318-327.
25. Lynch G, Baudry M. Brain spectrin, calpain and long-term changes in synaptic efficacy. Brain Research Bulletin. 1987;18(6):809-815.
26. Nptn - Neuroplastin precursor - Mus musculus (Mouse) - Nptn gene & protein [Internet]. Uniprot.org. 2021 [cited 17 June 2021]. Available from: https://www.uniprot.org/uniprot/P97300
27. Largo-Barrientos P, de Strooper B, Spires-Jones T, de Wit J, Uytterhoeven V, Verstreken P. Loss of synaptogyrin-3 rescues tau-induced memory defects and synaptic loss in the presence of microglial activation. Alzheimer's & Dementia. 2020;16(S3).
28. Baumgartel K, Mansuy I. Neural functions of calcineurin in synaptic plasticity and memory. Learning & Memory. 2012;19(9):375-384.
29. Gripap1 - GRIP1-associated protein 1 - Mus musculus (Mouse) - Gripap1 gene & protein [Internet]. Uniprot.org. 2021 [cited 17 June 2021]. Available from: https://www.uniprot.org/uniprot/Q8VD04
30. Roome C, Empson R. Assessment of the Contribution of the Plasma Membrane Calcium ATPase, PMCA, Calcium Transporter to Synapse Function Using Patch Clamp Electrophysiology and Fast Calcium Imaging. Methods in Molecular Biology. 2010;:343-360.
31. Gottschling C, Wegrzyn D, Denecke B, Faissner A. Elimination of the four extracellular matrix molecules tenascin-C, tenascin-R, brevican and neurocan alters the ratio of excitatory and inhibitory synapses. Scientific Reports. 2019;9(1).
32. Suire C, Abdul-Hay S, Sahara T, Kang D, Brizuela M, Saftig P et al. Cathepsin D regulates cerebral Aβ42/40 ratios via differential degradation of Aβ42 and Aβ40. Alzheimer's Research & Therapy. 2020;12(1).
33. Udayar V, Buggia-Prévot V, Guerreiro R, Siegel G, Rambabu N, Soohoo A et al. A Paired RNAi and RabGAP Overexpression Screen Identifies Rab11 as a Regulator of β-Amyloid Production. Cell Reports. 2013;5(6):1536-1551.
34. Mrschtik M, Ryan K. Lysosomal proteins in cell death and autophagy. FEBS Journal. 2015;282(10):1858-1870.
35. McLeod, F., Marzo, A., Podpolny, M., Galli, S. and Salinas, P., 2017. Evaluation of Synapse Density in Hippocampal Rodent Brain Slices. *Journal of Visualized Experiments*, (128).

36. Gross, A., Schoendube, J., Zimmermann, S., Steeb, M., Zengerle, R. and Koltay, P., 2015. Technologies for Single-Cell Isolation. *International Journal of Molecular Sciences*, 16(8), pp.16897-16919.